Editors' Suggestion

Magnetic-field periodic quantum Sondheimer oscillations in thin-film graphite

Toshihiro Taen ,* Andhika Kiswandhi , and Toshihito Osada

The Institute for Solid State Physics, The University of Tokyo, Kashiwa, Chiba, 277-8581, Japan

(Received 12 September 2023; revised 9 November 2023; accepted 21 November 2023; published 7 December 2023)

Materials with mesoscopic scales have provided an excellent platform for quantum-mechanical studies. Among them, the periodic oscillations of electrical resistivity against the direct and the inverse of magnetic fields, such as the Aharonov-Bohm effect and the Shubnikov-de Haas effect, manifest the interference of the wave function relevant to the electron motion perpendicular to the magnetic field. In contrast, the electron motion along the magnetic field also leads to the magnetic-field periodicity, which is the so-called Sondheimer effect. However, the Sondheimer effect has been understood only in the framework of the semiclassical picture, and thereby its interpretation at the quasiquantum limit was not clear. Here, we show that thin-film graphite exhibits clear sinusoidal oscillations over a wide range of the magnetic fields, where conventional quantum oscillations are absent. In addition, the sample with a designed step in the middle for eliminating the stacking disorder effect verifies that the period of the oscillations is inversely proportional to the thickness, which supports the emergence of the Sondheimer oscillations in the quasiquantum limit. These findings suggest that the Sondheimer oscillations can be reinterpreted as inter-Landau-level resonances. Our results expand the quantum oscillation family and pave the way for the exploration of the out-of-plane wavefunction motion.

DOI: 10.1103/PhysRevB.108.235411

I. INTRODUCTION

Oscillatory transport behavior under a magnetic field is a hallmark of the quantum transport property. For example, the Shubnikov-de Haas oscillations (SdHOs) have been explored in a wide class of semimetals or semiconductors [1–3], in which the electrical conductivity periodically oscillates against the inverse of the magnetic field. In contrast to the SdHOs, the Aharonov-Bohm (AB) effect [4–7] is known as a prototypical example of the direct magnetic-field periodic oscillations [8,9]. These quantum transport features stem from the wave nature of electrons along the path perpendicular to the magnetic field through quantizations or interferences. On the other hand, such an oscillatory behavior associated with the electron motion along the magnetic field was absent, since the electron motion along the magnetic field is, in principle, not influenced. Exceptional examples were found in very clean systems with a long mean free path, such as metallic or semiconducting crystals [10–16], mesoscopic-scale systems [17,18], and the surface of a topological insulator [19], in which clear magnetic-field-periodic oscillations are observed. These oscillations are known as the Sondheimer effect [20], which is determined by the "extra" momentum of the helical motion in a finite length scale (thickness of the film), and can be simply understood as a semiclassical effect [11,21].

Bernal-stacked graphite [Fig. 1(a)] provides an ideal platform in the study of the thickness-dependent features since it has a simple layered structure of two-dimensional carbon sheets (graphene) and hence we can easily obtain a sample with a well-defined thickness without any surface reconstructions. Moreover, the structural disorder is small enough to study the quantum transport properties. In fact, the mobility of the graphene isolated from graphite crystals is outstanding, which is experimentally demonstrated in state-of-the-art devices such as electron interferometers [22–28] as well as the confirmation of the hydrodynamic flow [28–32]. Remarkably, its low carrier concentration enables us to reach the so-called quasiquantum limit at an accessible magnetic field (around 8 T perpendicular to the plane), where only two Landau levels (LLs) remain at the Fermi level [33]. In this quasiquantum limit, the motion of carriers can no longer be treated in the semiclassical picture.

Here, we present clear sinusoidal oscillations in a graphite thin film, which is periodic in the magnetic field in the quasiquantum limit over a wide range of the magnetic fields (from around 10 T to 30 T). This is clearly distinct from the Shubnikov-de Haas oscillations, showing a periodic oscillation against the inverse of the magnetic field. We propose quantum Sondheimer effect as a cause of this magnetic-field periodicity. The model is developed by extending the semiclassical Sondheimer picture to the quasiquantum limit, where only two Landau levels with discretized energy level owing to quantum size effect are considered. In contrast to the typical magnetic-field periodic oscillations attributed to the in-plane carrier motion, such as the Aharonov-Bohm effect, the quantum Sondheimer effect arises from the out-of-plane motion and its period is inversely proportional to the sample thickness. Our experimental results show an excellent agreement with this relation, and verifies the realization of a new family of the quantum oscillations.

In our study, we prepared thin-film graphite mechanically exfoliated from Kish graphite crystals, followed by transfer onto a Si/SiO_2 substrate, electron-beam lithography, and a

*taen@issp.u-tokyo.ac.jp

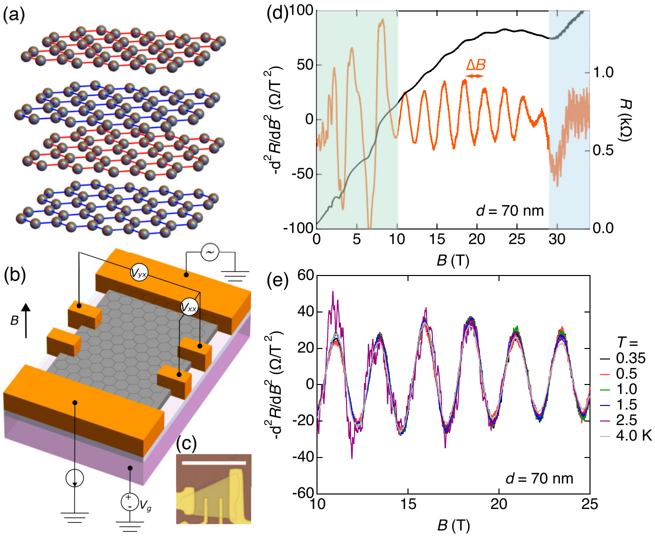

FIG. 1. (a) Schematic crystal structure of Bernal-stacked graphite. (b) Schematic of the thin-film graphite device. Transverse resistance ($R = V/I$) was measured by sweeping the magnetic fields (B) applied perpendicular to the film. (c) Optical microscopy image of device 1 ($d = 70$ nm); scale bar, 50 μm. (d) Magnetic field dependence of the transverse resistance R and its second derivative with respect to the magnetic field. At low magnetic fields (green shaded region), the SdHOs periodic in the inverse of the magnetic fields are observed. Above 30 T, the system is in the insulating density-wave phase (blue shaded region). In between, in 10 − 30 T, clear B-periodic resistivity oscillations are observed. (e) The oscillatory components of the resistance estimated by the second derivative between 10 and 25 T at different temperatures.

deposition of Cr/Au contact to form the field-effect transistors [Figs. 1(b) and 1(c)]. A heavily doped silicon substrate was used for applying gate voltage V_g, which did not play an important role in the present study. Each sample thickness was determined by AFM analyses. A typical sample dimension is around 50×50 μm^2 in the plane, and a thickness is of the order of 100 nm. The thickness is over a hundred times larger than the out-of-plane lattice constant, where the quantum size effect plays an important role [34,35]. The sample was cooled down to 0.35 K by using a helium-3 refrigerator, and the transverse magnetoresistance up to 35 T was measured, as detailed previously [35]. The in-plane electrical resistance R was measured by dc method with reversing a constant current or lock-in technique under a magnetic field B along the c axis. High magnetic fields were generated in a 35 T resistive magnet at the National High Magnetic Field Laboratory.

Figure 1(d) represents the magnetoresistance in the thin-film graphite with a thickness of 70 nm. Below 8 T, the SdHO patterns are the same as that in bulk crystals [33], which demonstrates that the three-dimensional band dispersion still holds.

II. MAGNETIC-FIELD-PERIODIC RESISTIVITY OSCILLATIONS

In a bulk semimetal or semiconductor, any anomalous transport behavior is not expected between the SdHOs unless many-body effects play a crucial role. In fact, once the system goes into the quasiquantum limit at around 8 T, where the LL with an index $N = 1$ escapes from the Fermi energy and no quantum oscillations occur up to 53 T [36–38], the bulk graphite does not exhibit any notable structure in the magnetoresistivity before entering the electron-interaction-induced phase transition at around 30 T [37,39–41] [Fig. 1(d)]. However, our thin-film graphite shows a clear oscillatory behavior with a single period $\Delta B \approx 2.5$ T in a wide range of magnetic fields from 10 T to 30 T, as shown in Fig. 1(d). Although it is difficult to resolve it owing to the large SdHOs, the present oscillations might coexist below 10 T in the thin film. As we measured in a different thickness sample, the period of the oscillations has different values. For example, device 2 with $d = 178$ nm has a smaller period of $\Delta B \approx 1$ T [35]. As shown in Fig 1(e), the period and the amplitude, as well as the phase, are almost unchanged below 4 K. In the case of the multilayer graphene stacking with a magic twist angle, correlated effects, such as the superconductivity, are fragile above 4 K [42–44]. This implies that the present temperature-insensitive oscillations observed in the less confined graphite samples than graphene are not attributable to the many-body effect.

III. SEMICLASSICAL AND QUANTUM SONDHEIMER EFFECT

Magnetic-field-periodic oscillations are often attributed to the Aharonov-Bohm (AB) effect [4,5,7]. The AB effect originates from the interference between two wave functions propagating along different paths in a ringlike structure (the so-called AB ring). The AB effect emerges, for example, in the artificially designed ring shaped or regularly patterned antidots two-dimensional (2D) devices [45,46]. Hence, for the appearance of the AB effect, there must exist an AB ring orthogonal to the magnetic field in the current three-dimensional (3D) sample. One possible origin is the formation of the moiré superlattice at the stacking faults [47]. The lattice mismatch arising from the misalignment at the stacking faults leads to the potential variations with a mesoscopic scale, imposing an interference in the twisted graphene systems [48]. In this case, however, only the interface would be responsible for the conductance oscillations, which might be masked by the majority part of the bulk.

Another possible origin of the magnetic field periodicity is the Sondheimer effect. The Sondheimer effect has been explained in the semiclassical picture, and experimentally observed in clean thin films [17,18]. The semiclassical pictures are schematically illustrated in Figs. 2(a) and 2(b). As the magnetic field B is applied orthogonal to the conducting thin film with a thickness d, the charged carrier (red ball) moves along the helical orbit (blue solid curve), which is composed of an out-of-plane free motion and an in-plane cyclotron motion. The out-of-plane motion with a velocity of $v_{F,z}$ is not perturbed by the magnetic fields, whereas the in-plane cyclotron motion is determined by the strength of the magnetic field B through the angular frequency of $\omega_c = eB/m_{\rm cyc}$, where e is the elementary charge and $m_{\rm cyc}$ is the effective cyclotron mass. As a result, the helical orbit has the same periodicity as the cyclotron motion with a time period $T = 2\pi/\omega_c$. Provided that the system is free from any scattering in the

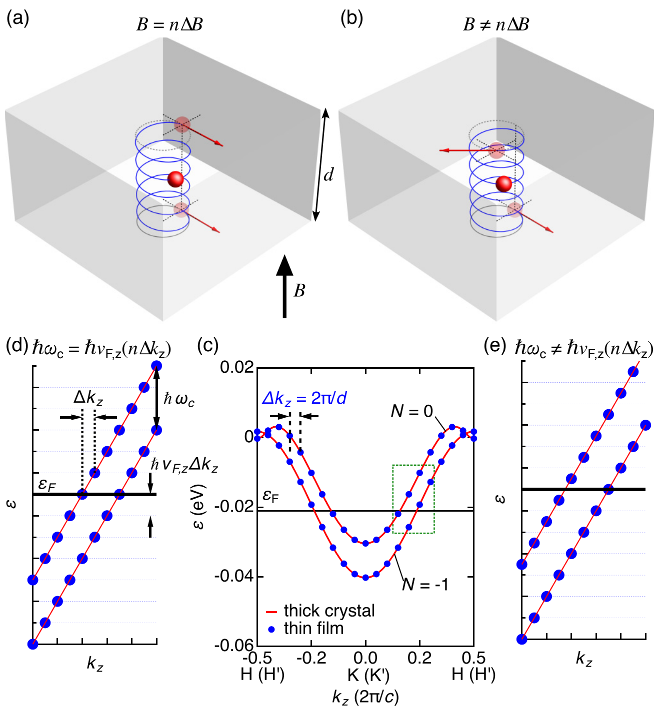

FIG. 2. (a), (b) Schematics of the semiclassical picture of the Sondheimer effect. The magnetic field B is applied perpendicular to the plane equal to an integer (n) multiple of ΔB (a) and not equal to it (b) for a clean-limit thin film with a thickness of d. Under the magnetic field, the carrier (red ball) moves along the helical orbit (blue curve). At the condition $B = n\Delta B$ (a), the integer multiple of the helical-motion period fits perfectly into the film (the black dotted cross at the top surface is located exactly above the one at the bottom). (c) The dispersion of LLs for graphite along k_z at the quasiquantum limit. At the quasiquantum limit ($B > 7.4$ T perpendicular to the plane), only $N = 0$ and -1 LLs remain on the Fermi level ε_F. In contrast to a thick system (conventional crystal), where the dispersion is continuous (red curves), k_z in thin film is discretized owing to the quantum size effect with a reciprocal-lattice spacing of $\Delta k_z = 2\pi/d$ (blue solid markers). (d), (e) The quantum interpretation of the Sondheimer effect. The figures are magnified views of the dashed green rectangle in Fig. 2(c). The condition Eq. (2) is satisfied in Fig. 2(d), while not in Fig. 2(e).

bulk, the carrier travels from the bottom to the top (or vice versa) over a time span of $d/v_{F,z}$. At some special magnetic fields [Fig. 2(a)], this time span becomes equal to the integer multiple of T; $d/v_{F,z} = nT$, where n is an integer. We refer to this special condition as the Sondheimer condition. This Sondheimer condition is periodically satisfied with a period ΔB, which is expressed as [11,21]

$$\Delta B = \frac{2\pi}{ed} m_{\mathrm{cyc}} v_{F,z} \propto 1/d. \tag{1}$$

The magnetoconductivity varies in accordance with the Sondheimer condition fulfilled. It is noteworthy that the period ΔB of the Sondhemier effect is inversely proportional to the film thickness d. The Sondheimer effect is in stark contrast to the AB effect for its bulk nature. In other words, the Sondheimer is innately a 3D feature since it arises from the out-of-plane motion. However, the validity of this picture seems limited only in the semiclassical regime, namely a substantial number of the LLs participate in the formation of the wave packets representing the charged carrier in helical motion [red ball in Fig. 2(a)]. In fact, the Sondheimer effect was treated in the framework of the Boltzmann's theory [11,21].

The magnetic-field periodic oscillations in our graphite thin-film appear in the quasiquantum limit, where only two LLs with the indices of $N = -1$ and 0 remain on the Fermi level. The labels of these indices are in accordance with the convention. Here, the semiclassical picture is no longer applicable since we cannot compose the particle nature only from the two LLs. After translating the semiclassical Sondheimer effect formula into the quantum one, we obtain the condition of the quantum Sondhemier effect as follows:

$$\hbar\omega_c = \hbar v_{F,z}(n\Delta k_z). \tag{2}$$

Here, $\hbar = h/2\pi$ is the Planck constant divided by 2π, k_z is the wave number along the direction perpendicular to the plane, $v_{F,z} = (1/\hbar)d\varepsilon/dk_z$ is the Fermi velocity along the k_z, ε is the energy band dispersion, $\Delta k_z = 2\pi/d$ is the interval of the k_z points, and n is an integer. Note that Δk_z is a considerable magnitude for around 100-nm-thick graphite [34,35]. We emphasize that Eq. (2) is mathematically equivalent to the semiclassical formula Eq. (1), but is expressed in the quantum formalism. This reformulation leads to the quantum interpretation of the Sondheimer effect at the quasiquantum limit, as shown in Figs. 2(c)–2(e). We will only consider $N = -1$ and 0 LLs at the quasiquantum limit in graphite as a special case. The generalized case is given in Appendix A. There are two characteristic energy scales in this situation; the cyclotron energy $\hbar\omega_c$ and the discretized energy separation $\hbar v_{F,z}\Delta k_z$ [Fig. 2(d)]. The energy separation between the LLs is characterized by the cyclotron energy $\hbar\omega_c$, which is proportional to the magnetic fields. Each LL is evenly discretized along the k_z direction with an interval of Δk_z owing to the quantum size effect, which is solely determined by the thickness and not affected by the magnetic fields. This discretization corresponds to a standing wave condition along the z direction. The limitation on the allowed k_z mode leads to the discretized energy levels around the Fermi energy ε_F with an energy gap of $\Delta k_z(d\varepsilon/dk_z)|_{\varepsilon=\varepsilon_F} = \hbar v_{F,z}\Delta k_z$. This separation of the discretized energy levels becomes sizable only in thin film having largely dispersive bands. With increasing magnetic field, only the upper $N = 0$ LL shifts upwards, whereas the $N = -1$ stays behind [49]. A point in the discretized level belonging to $N = 0$ LL is horizontally aligned to that in the other $N = -1$ LL around the Fermi level when the condition of Eq. (2) is satisfied, namely the cyclotron energy is equal to the integer multiple of the discretized energy level separation. This overlap of the discretized energy levels leads to the resonant inter-LL scattering conserving the energy and the spin of the carriers. The magnetoconductivity enhancement at the resonance condition is approximately proportional to the form of $\Gamma/(\Delta E^2 + (2\Gamma)^2)$, which corresponds to the semiclassical picture depicted in Figs. 2(a) and 2(b), where ΔE and Γ are the energy difference between the energy levels responsible for the resonance and the energy level broadening, respectively. Consequently, the semiclassical Sondheimer effect can be reinterpreted as the quantum Sondheimer effect at the quasiquantum limit. (See Appendix B for the spin degrees of freedom).

The direct evidence of the quantum Sondheimer effect is the relation $\Delta B \propto 1/d$ at the quasiquantum limit. In order to confirm this relation, the most simple method is to prepare several samples having various thicknesses and explore the oscillation periods. However, the results obtained from different samples need to be carefully compared, since they might include unintentional differences, for example, the amount of disorder. In the present case, stacking faults would play a crucial role, since those defects obstruct the helical motion. Although the layered structure of graphite is beneficial to obtain a well-defined thickness, it is prone to include the stacking faults [47] as a drawback. The stacking faults segmentize the thickness and break the periodic condition along the out-of-plane direction, which inhibits the formation of standing waves over the full thickness of the film. This implies a possible dissociation between the real thickness of the film and the effective thickness responsible for the observed oscillations.

In order to avoid ambiguity in the effective thickness, we designed the sample that enables us to investigate the thickness dependence in a single sample, as shown in Figs. 3(a) and 3(b). The sample has a step in the middle, which is accidentally formed during the mechanical exfoliation process. The step divides the sample into the thinner region (right part) and the thicker region (left part) with a thickness of $d_{\rm thin}$ and $d_{\rm thick}$, respectively. The thicknesses of the thinner and thicker region in our device were determined from the atomic-force microscopy (AFM) as shown in Figs. 3(c) and 3(d) as $d = 63$ nm and $d = 85$ nm, respectively. It is natural to assume that the stacking faults, such as twisted interface, were formed at the crystal growth, so the microcrystal for the device, which is exfoliated from the as-grown crystal, includes those stacking faults over its whole region [Fig. 3(e)]. On the other hand, in the mechanical exfoliation process, the edge parts of the microcrystal are subject to the force to peel off layers, which could introduce planar cracks that are concentrated at the edge. Most of these planar cracks are expected to disappear since the two layers across the planar cracks can combine via the van der Waals interaction as long as the gap of the cracks is small enough not to be wedged by obstacles. A small number of remaining cracks might have no effect on the transport properties since they exist only at the sample edges.

If the sample includes a stacking fault over its entire region, as shown in Fig. 3(e), both the thinner and thicker regions would have reduced effective thicknesses, denoted as $d^{\rm eff}_{\rm thin}(<d_{\rm thin})$ and $d^{\rm eff}_{\rm thick}(< d_{\rm thick})$, respectively. In the case of Fig. 3(e), even if we cannot determine the absolute values of these effective thicknesses, the trend of the thickness-dependent transport features can be detected since the thickness relation holds ($d^{\rm eff}_{\rm thin} < d^{\rm eff}_{\rm thick}$). Another possible configuration is shown in Fig. 3(f), where a stacking fault only exists in the bump region. Even in this case, although the thickness difference between thinner and thicker parts becomes small or zero, the relation is not inverted ($d^{\rm eff}_{\rm thin} \leqslant d^{\rm eff}_{\rm thick}$). As a result, the trend of thickness dependence of the transport property can be observed by using this step-structure sample even if the stacking faults are included.

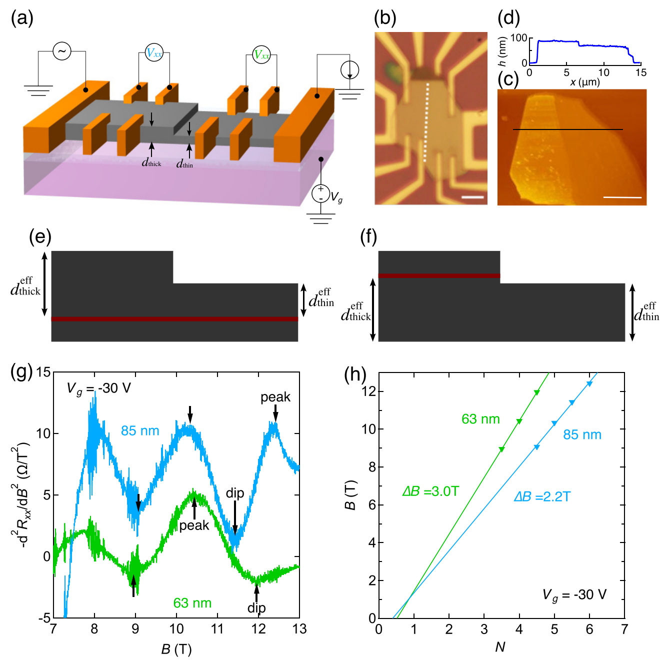

FIG. 3. (a) Schematic setup of the device with a step in the middle. The thicknesses of the left and right part is $d_{\rm thick}$ and $d_{\rm thin}$, respectively. (b), (c) The optical micrography (b) and atomic-force micrography (c) image of the device, respectively. The step is highlighted in a white broken line in Fig. 3(b). The scale bars, 5μm. (d) The line profile along the black line in Fig. 3(c). (e), (f) The schematic side views of the sample with a stacking fault (red line). If the system is scattering free except at the stacking fault, the effective thicknesses of the thick and thin parts are reduced to $d^{\rm eff}_{\rm thick}$ and $d^{\rm eff}_{\rm thin}$, respectively. (g) The magnetic-field periodic oscillations for the thin (light green) and thick (light blue) parts for $B = 7 - 13$ T. The oscillatory components is extracted by the second derivative d^2R_{xx}/dB^2. The bottom gate voltage $V_g = -30$ V is applied. Other V_g data give almost the same results. The peak and dip positions are marked by arrows. (h) The estimation of the period of the oscillations. By assigning the peak and dip magnetic-field values to the integers and half integers, respectively, the periods ΔB of the magnetic-field periodic oscillations for thin and thick parts are estimated from the slope of the linear fit as 3.0 T and 2.2 T, respectively.

The observed resistance oscillations (d^2R_{xx}/dB^2) for the thinner (green curve) and the thicker regions (light blue curve) are plotted in Fig. 3(g). As expected from the quantum Sondheimer effect [$\Delta B \propto 1/d$, Eq. (1)], a larger period is identified in the thinner part of the sample. By assigning the peaks and the dips to integers and half integers, respectively, the period of each region is determined, as shown in Fig. 3(h). The slope of the fitting line yields the period of the magnetic-field-periodic oscillations, with the value of $\Delta B = 3.0$ T and 2.2 T for $d = 63$ nm and 85 nm regions, respectively. The ratio of the periods $3.0/2.2 \approx 1.36$ is in good agreement with the inverse-thickness ratio $85/63 = 1.35$, which is consistent with the quantum Sondheimer effect. Note that this quantitative agreement suggests that the stacking faults are absent in this device.

The relation between the period ΔB and the inverse of the thickness $1/d$ is summarized in Fig. 4(a) (orange diamonds).

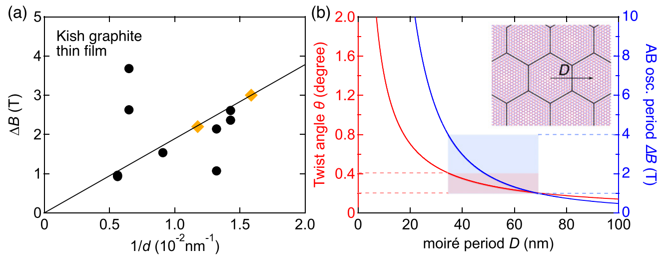

FIG. 4. (a) Experimentally observed magnetic-field periods as a function of the inverse of the thickness $1/d$. Orange diamond markers are from the device with a step. The solid line is the guide to the eye. (b) The consideration of the AB effect scenario. The moiré period D (bottom axis) is determined by the twist angle θ (left axis) through the formula $D = a/(2\sin(\theta/2))$ (red line). By assuming the area of the moiré unit cell S enclosed by an AB ring, the AB oscillation period ΔB (right axis) is expressed as $\Delta B = \phi_0/S$ (blue line). In order to assign the experimentally observed oscillations to the AB oscillations, the moiré period should be 35-69 nm, which corresponds to the limited range of the twist angle $\theta \approx 0.2$-$0.4\,^\circ$. The inset indicates the moiré superlattice formed at the stacking fault with a moiré period D.

The periods obtained from step-free samples [35] are also displayed (black solid circles). Regardless of the sample qualities, almost all the data points fall onto the line determined by the sample with a step, which is presumably free from the stacking faults. The consistent linear relation between ΔB and $1/d$ indicates that the magnetic-field-periodic oscillations in the quasiquantum limit are attributable to the quantum Sondheimer effect. Although multiple periods with exceptionally large values are found in the sample with $d = 154$ nm ($1/d = 0.65 \times 10^{-2}$ nm^{-1}), the result is reasonably explained by the segmentation of the thickness by the stacking faults. If we assume that each segmented part produces the oscillations, the observed periods are well explained by the same line in Fig. 4(a), supporting the quantum Sondheimer effect scenario.

IV. DISCUSSION

Our results indicate that the AB effect originating from the superlattice at the stacking-fault interface is unlikely to emerge. First, only a very narrow range of the twist angle θ is possible to explain the observed oscillations period. The moiré period D [the period of the so-called AA stacking region, inset of Fig. 4(b)] formed at the stacking fault of graphite is determined solely by the twist angle through the equation $D = a/(2\sin(\theta/2))$ [red curve in Fig. 4(b)], where a is the in-plane lattice constant of the graphite. On the other hand, the AB oscillations period ΔB is determined by the area S enclosed by the AB ring through the equation $\Delta B = \phi_0/S$, where $\phi_0 = h/e$ is the magnetic flux quantum. By assuming that each moiré unit cell [hexagonal cell enclosed by black solid lines in the inset of Fig. 4(b)] works as a unit of an AB ring, S can be represented with moiré period D through the equation $S = \sqrt{3}D^2/2$, namely the AB oscillations period ΔB is determined by the moiré period D [blue curve in Fig. 4(b)]. If the observed magnetic-field-periodic oscillations with a period of $\Delta B = 1$-4 T are attributed to the AB effect, the value of the moiré period should be $D \approx 35$-69 nm [blue shade in Fig. 4(b)]. This moiré period can be translated into the twist angle at the stacking fault as $\theta \approx 0.2^\circ$-0.4° [red shade in Fig. 4(b)]. Since the twist angle at the stacking fault should have a random value, it is very unnatural to assume that only a very limited range of twist angles are formed. In other words, random ΔB values should be observed if it was due to the AB effect mechanism. Although the AB-ring area S would be quantitatively different from the current estimation when the crystal reconstruction at the interface occurs, it is difficult to reproduce such a limited range of oscillation periods by using the AB effect scenario.

V. SUMMARY AND OUTLOOK

Finally, we summarize the necessary condition to observe the quantum Sondheimer effect. First, a clean bulk with a well-defined thickness is necessary. This condition was realized in a clean semimetal fabricated using a focused-ion beam method [17], but it is easily satisfied in layered materials. Second, the energy spacing arising from the quantum size effect $\hbar v_{F,z}\Delta k_z$ needs to be resolved. This condition requires a large Fermi velocity $v_{F,z} = (1/\hbar)d\varepsilon/dk_z$, i.e., a large bandwidth. Third, only a few LLs should remain at the Fermi level at the accessible magnetic fields in order to reach the quantum Sondheimer regime. In the graphite case, only two LLs remain above $B = 7.4$ T neglecting the spin degrees of freedom. As a result, graphite thin film turns out to be an ideal platform to satisfy these conditions. The quantum Sondheimer effect should be generically observed as long as these conditions are satisfied. Even below the quasiquantum limit, a more complicated quantum Sondheimer effect with multiple resonant conditions is expected, which would be observed when the SdHOs are killed with elevating temperatures. The combination with other electronic states, such as the density-wave state, could offer new paths to explore the novel physics in quantum devices.

ACKNOWLEDGMENTS

The authors acknowledge Dr. E.S. Choi for technical support and discussions. A portion of this work was performed at the National High Magnetic Field Laboratory, which is supported by National Science Foundation Cooperative Agreement No. DMR-1157490 and the state of Florida. This work was partially supported by JSPS KAKENHI Grants No. JP15K21722, No. JP25107003, No. JP16H03999, No. JP16K17739, No. JP19K14655, No. JP22K03523, and No. JP23K03297.

APPENDIX A: GENERAL CASE OF THE QUANTUM SONDHEIMER EFFECT

At the quasiquantum limit in graphite, only two LLs of $N = 0$ and $N = -1$ remain at the Fermi energy. Moreover, since the $N = -1$ LL is insensitive to the magnetic field, it is easy to derive the Sondheimer condition Eq. (2). Here we will consider the general case, where an arbitrary number of LLs exist with an equal energy spacing $\hbar\omega_c$. The key concept of the quantum Sondheimer effect arises from the resonant states

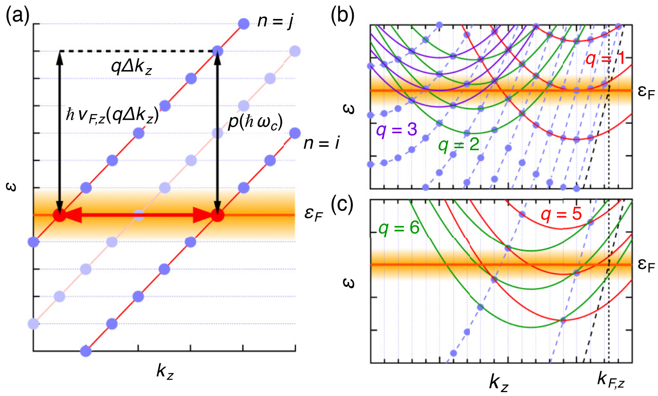

FIG. 5. The general case of the quantum Sondheimer effect. (a) The resonant pair (red markers) on the Fermi energy ε_F with $p = j - i$, and q associated with the quantum Sondheimer effect. The band dispersions are approximated with a linear one. (b), (c) The Sondheimer subbands (solid lines) under lower (b) and higher (c) magnetic fields on the basis of Landau subbands for the free electron model [Eq. (A2), broken blue lines]. Only the Sondheimer subbands with $p = 1$ are shown.

among the discretized energy levels belonging to different Landau indices. Suppose the resonant pair is found between the LLs indexed by $N = i$ and $N = j = i + p$ [Fig. 5(a)], where the integer $p = j - i \geqslant 1$ indicates the Landau index difference. At one k_z, the energy difference between the discretized levels belonging to $N = i$ and that to $N = j$ is equal to $p(\hbar\omega_c)$. In addition, another integer $q \geqslant 1$ is introduced so as to minimize the energy difference $p(\hbar\omega_c) - \hbar v_{F,z} q\Delta k_z$, where the Fermi velocity along the k_z direction, $v_{F,z}$ gives the slope of the Landau subband through $\hbar v_{F,z}$. If this energy difference goes zero, a resonant pair is formed [red markers in Fig. 5(a)]. As a result, the general formulation of the quantum Sondheimer effect is described as

$$\frac{p}{q}\hbar\omega_c = \hbar v_{F,z}\Delta k_z. \tag{A1}$$

For each Landau-level configuration, multiple resonant modes indexed by a ratio $p/q > 0$ are allowed. The quasiquantum limit is the special case, where at most one resonant mode ($p/q = 1/n$) survives at a fixed magnetic field [Eq. (2)].

In order to unify the quantum and the semiclassical pictures, the fully quantum calculation of the conductivity is required in the semiclassical regime, which is beyond the scope of this paper. Instead, hereafter we will see a trace of the semiclassical characteristics by using the quantum picture. In the semiclassical Sondheimer picture, illustrated in Figs. 2(a) and 2(b), the dominating contributions for the oscillatory part of the conductivity $\Delta\sigma$ arise from the local Gaussian curvature of the Fermi surface at the limiting points (extreme k_z) for the elliptic Fermi surface [11,12,21]. The Landau quantization and the concomitant quantum Sondheimer resonance are considered in the situation where substantial Landau levels exists. For simplicity, we focus on the free electron model, where each LL dispersion is written as

$$\varepsilon_N(k_z) = \left(N + \frac{1}{2}\right)\hbar\omega_c + \frac{\hbar^2 k_z^2}{2m}. \tag{A2}$$

By introducing the quantum size effect, k_z is discretized with a unit of $\Delta k_z = (2\pi)/d$. The discretized Landau subbands for lower and higher magnetic fields are shown in Figs. 5(b) and 5(c), respectively [blue broken lines are the guide of Eq. (A2)]. The conventional quantum oscillations arise from the bottom of these Landau subbands passing through the Fermi energy ε_F. In addition to the Landau subbands, other subbands (referred to as the Sondheimer subbands), exemplified by solid lines, are visualized in Figs. 5(b) and 5(c). For a substantial number of LLs, a series of p/q Sondheimer subbands satisfies the Sondheimer condition Eq. (A1). The analytical expression of the solid lines in Figs. 5(b) and 5(c) is

$$\varepsilon^{(p/q)}_{\{N_0,j\}}(k_z) = \left(N_0 + \frac{1}{2} + j\frac{p}{q}\right)\hbar\omega_c + \frac{\hbar^2}{2m_z}\left(k_z - k^{(p/q)}_{z,\min}\right)^2 - \frac{\hbar^2}{2m_z}\left(k^{(p/q)}_{z,\min}\right)^2, \tag{A3}$$

where j is an integer such that $0 \leqslant j \leqslant q - 1$, m_z is the effective mass along the z direction, $k^{(p/q)}_{z,\min} = \frac{p}{q}\frac{deB}{2\pi\hbar} = \frac{p}{q}\frac{1}{(\hbar^2/2m_z)\Delta k_z}\frac{\hbar\omega_c}{2}$ is the wave number giving the Sondheimer subband minimum, and $\{N_0, j\}$ is the Sondheimer subband indices. It is noteworthy that the minimum location $k^{(p/q)}_{z,\min}$ for each p/q mode linearly shifts toward higher k_z by sweeping up the magnetic fields [Fig. 5(c)]. If both consecutive points

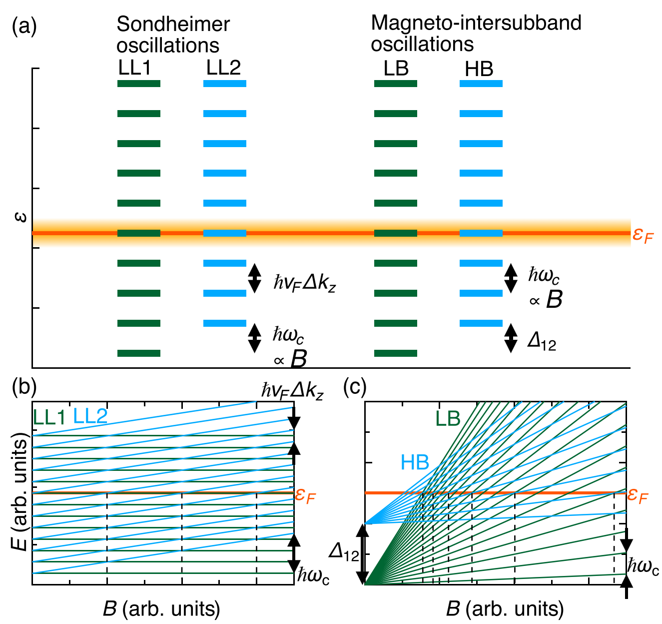

FIG. 6. Comparison between the quantum Sondheimer oscillations and the MIS oscillations. (a) Subband configurations. In the Sondheimer effect, two discretized Landau levels [LL1 and LL2 ($N = -1$ and $N = 0$ in graphite, respectively)] with an interval of $\hbar v_F\Delta k_z$ have an energy offset, linearly increasing with the magnetic field. In MIS oscillations, on the other hand, the energy spacing of the lower-energy band (LB) and the higher-energy band (HB) linearly increases with the magnetic field with a fixed offset Δ_{12}. (b), (c) The magnetic-field evolution of the discretized levels [shown in Fig. 6(a)] for the Sondheimer oscillations (b) and the MIS oscillations (c). The resonant condition (vertical dashed lines) appears periodically in B and $1/B$ for the Sondheimer and the MIS oscillations, respectively.

in one p/q subband locate together around the Fermi energy, then p/q mode satisfies the Sondheimer condition Eq. (A1). Therefore, only the p/q modes satisfying $k_{z,\min}^{(p/q)} < k_{\mathrm{F},z}$ are relevant. Among these modes, the largest p/q mode, which gives the largest $k_{z,\min}^{(p/q)}$, plays a main role, since it is the first one to be excluded from them by increasing the magnetic field. Every time the largest p/q mode goes beyond the limiting point, namely $k_{z,\min}^{(p/q)} \gtrsim k_{\mathrm{F},z}$, the contribution of that p/q mode is eliminated from the sum of the resonant modes. This quantum picture emphasizes the importance of the behavior around the limiting point, which corresponds to the semiclassical picture.

APPENDIX B: SPIN DEGREES OF FREEDOM

We discuss the quantum Sondheimer effect in graphite by neglecting the spin degrees of freedom. In the realistic band structure of graphite, there are four spin-split Landau bands at the quasiquantum limit: $(N=0,\uparrow)$, $(N=0,\downarrow)$, $(N=-1,\uparrow)$, and $(N=-1,\downarrow)$. However, this spin splitting is not important since the resonance condition requires the coupling between the energy and spin conserved states. The spin degrees of freedom can be taken into account by considering two distinctive pairs of $(N=0,\uparrow) \leftrightarrow (N=-1,\uparrow)$ and $(N=0,\downarrow) \leftrightarrow (N=-1,\downarrow)$.

APPENDIX C: COMPARISON TO MAGNETOINTERSUBBAND OSCILLATIONS

It is interesting to compare the quantum Sondheimer oscillations and magnetointersubband (MIS) oscillations. The MIS oscillations arise when two series of Landau subbands [lower-energy band (LB) and higher-energy band (HB)] are formed under high magnetic fields. Here these two subbands have an energy offset Δ_{12} at zero magnetic field and are discretized with an equal energy interval of $\hbar\omega_c$ under the magnetic field. The energy intervals for both subbands increase proportionally to the magnetic field ($\hbar\omega_c \propto B$), and the two energy levels belonging to the opposite subband sequentially come in alignment with a period of the inverse of the magnetic field ($1/B$ periodic) [50,51]. Recently, the twisted bilayer graphene has been known to show the MIS oscillations under the interlayer displacement field [52].

By comparison, in the quantum Sondheimer effect, there are only two Landau levels (LL1 and LL2) with an energy offset of $\hbar\omega_c$ and each of them is discretized by the quantum size effect with a spacing of $\hbar v_F \Delta k_z$. This energy interval is solely determined by the thickness and the Fermi velocity and does not vary with the magnetic field, which is clearly distinct from the MIS oscillations. This different setup produces the magnetic-field periodicity in the Sondheimer oscillations, in contrast to $1/B$ periodicity in the MIS oscillations. These two setups are depicted in Fig. 6.

[1] S. B. Hubbard, T. J. Kershaw, A. Usher, A. K. Savchenko, and A. Shytov, Millikelvin de Haas–van Alphen and magnetotransport studies of graphite, Phys. Rev. B **83**, 035122 (2011).

[2] J. M. Schneider, B. A. Piot, I. Sheikin, and D. K. Maude, Using the de Haas–van Alphen effect to map out the closed three-dimensional fermi surface of natural graphite, Phys. Rev. Lett. **108**, 117401 (2012).

[3] D. Shoenberg, *Magnetic Oscillations in Metals*, Cambridge Monographs on Physics (Cambridge University Press, 1984).

[4] Y. Aharonov and D. Bohm, Significance of electromagnetic potentials in the quantum theory, Phys. Rev. **115**, 485 (1959).

[5] Y. Aharonov and D. Bohm, Further considerations on electromagnetic potentials in the quantum theory, Phys. Rev. **123**, 1511 (1961).

[6] R. G. Chambers, Shift of an electron interference pattern by enclosed magnetic flux, Phys. Rev. Lett. **5**, 3 (1960).

[7] A. Tonomura, N. Osakabe, T. Matsuda, T. Kawasaki, J. Endo, S. Yano, and H. Yamada, Evidence for Aharonov-Bohm effect with magnetic field completely shielded from electron wave, Phys. Rev. Lett. **56**, 792 (1986).

[8] A. Bachtold, C. Strunk, J.-P. Salvetat, J.-M. Bonard, L. Forró, T. Nussbaumer, and C. Schönenberger, Aharonov–Bohm oscillations in carbon nanotubes, Nature (London) **397**, 673 (1999).

[9] S. Russo, J. B. Oostinga, D. Wehenkel, H. B. Heersche, S. S. Sobhani, L. M. K. Vandersypen, and A. F. Morpurgo, Observation of Aharonov-Bohm conductance oscillations in a graphene ring, Phys. Rev. B **77**, 085413 (2008).

[10] M. Toda, H. Tanaka, H. Kiyooka, and Y. Mizushima, Experimental verification of the Sondheimer-effect in thin metallic films, J. Phys. Soc. Jpn. **19**, 2353 (1964).

[11] J. A. Munarin, J. A. Marcus, and P. E. Bloomfield, Size-dependent oscillatory magnetoresistance effect in gallium, Phys. Rev. **172**, 718 (1968).

[12] P. D. Hambourger and J. A. Marcus, Size-dependent oscillatory magnetoresistance in cadmium, Phys. Rev. B **8**, 5567 (1973).

[13] I. Sakamoto, Sondheimer oscillation in copper, Phys. Lett. A **53**, 227 (1975).

[14] I. Sakamoto and T. Sato, Temperature dependence of electronic relaxation time in the Sondheimer size effect of copper, J. Low Temp. Phys. **36**, 79 (1979).

[15] H. Sato, Sondheimer oscillation in aluminium single crystals, Phys. Status Solidi B **94**, 309 (1979).

[16] H. Sato, Phonon-limited mean free path in the Sondheimer oscillation of aluminum, J. Low Temp. Phys. **38**, 267 (1980).

[17] M. R. van Delft, Y. Wang, C. Putzke, J. Oswald, G. Varnavides, C. A. C. Garcia, C. Guo, H. Schmid, V. Süss, H. Borrmann, J. Diaz, Y. Sun, C. Felser, B. Gotsmann, P. Narang, and P. J. W. Moll, Sondheimer oscillations as a probe of non-ohmic flow in WP_2 crystals, Nat. Commun. **12**, 4799 (2021).

[18] S. Mallik, G. C. Ménard, G. Saïz, I. Gilmutdinov, D. Vignolles, C. Proust, A. Gloter, N. Bergeal, M. Gabay, and M. Bibes, From low-field Sondheimer oscillations to high-field very large and linear magnetoresistance in a $SrTiO_3$-based two-dimensional electron gas, Nano Lett. **22**, 65 (2022).

[19] H.-J. Kim, K.-S. Kim, M. D. Kim, S.-J. Lee, J.-W. Han, A. Ohnishi, M. Kitaura, M. Sasaki, A. Kondo, and K. Kindo, Sondheimer oscillation as a signature of surface Dirac fermions, Phys. Rev. B **84**, 125144 (2011).

[20] E. H. Sondheimer, The influence of a transverse magnetic field on the conductivity of thin metallic films, Phys. Rev. **80**, 401 (1950).
[21] V. L. Gurevich, Oscillations in the conductivity of metallic films in magnetic fields, Sov. Phys. JETP **8**, 464 (1959).
[22] A. F. Young and P. Kim, Quantum interference and Klein tunnelling in graphene heterojunctions, Nat. Phys. **5**, 222 (2009).
[23] P. Rickhaus, R. Maurand, M.-H. Liu, M. Weiss, K. Richter, and C. Schönenberger, Ballistic interferences in suspended graphene, Nat. Commun. **4**, 2342 (2013).
[24] T. Taychatanapat, K. Watanabe, T. Taniguchi, and P. Jarillo-Herrero, Electrically tunable transverse magnetic focusing in graphene, Nat. Phys. **9**, 225 (2013).
[25] A. Varlet, M.-H. Liu, V. Krueckl, D. Bischoff, P. Simonet, K. Watanabe, T. Taniguchi, K. Richter, K. Ensslin, and T. Ihn, Fabry-Pérot interference in gapped bilayer graphene with broken anti-Klein tunneling, Phys. Rev. Lett. **113**, 116601 (2014).
[26] T. Machida, S. Morikawa, S. Masubuchi, R. Moriya, M. Arai, K. Watanabe, and T. Taniguchi, Edge-channel transport of Dirac fermions in graphene quantum Hall junctions, J. Phys. Soc. Jpn. **84**, 121007 (2015).
[27] D. S. Wei, T. van der Sar, J. D. Sanchez-Yamagishi, K. Watanabe, T. Taniguchi, P. Jarillo-Herrero, B. I. Halperin, and A. Yacoby, Mach-Zehnder interferometry using spin- and valley-polarized quantum Hall edge states in graphene, Sci. Adv. **3**, e1700600 (2017).
[28] Y. Ronen, T. Werkmeister, D. Haie Najafabadi, A. T. Pierce, L. E. Anderson, Y. J. Shin, S. Y. Lee, Y. H. Lee, B. Johnson, K. Watanabe, T. Taniguchi, A. Yacoby, and P. Kim, Aharonov–Bohm effect in graphene-based Fabry–Pérot quantum Hall interferometers, Nat. Nanotechnol. **16**, 563 (2021).
[29] D. A. Bandurin, I. Torre, R. K. Kumar, M. B. Shalom, A. Tomadin, A. Principi, G. H. Auton, E. Khestanova, K. S. Novoselov, I. V. Grigorieva, L. A. Ponomarenko, A. K. Geim, and M. Polini, Negative local resistance caused by viscous electron backflow in graphene, Science **351**, 1055 (2016).
[30] J. Crossno, J. K. Shi, K. Wang, X. Liu, A. Harzheim, A. Lucas, S. Sachdev, P. Kim, T. Taniguchi, K. Watanabe, T. A. Ohki, and K. C. Fong, Observation of the Dirac fluid and the breakdown of the Wiedemann-Franz law in graphene, Science **351**, 1058 (2016).
[31] R. Krishna Kumar, D. A. Bandurin, F. M. D. Pellegrino, Y. Cao, A. Principi, H. Guo, G. H. Auton, M. Ben Shalom, L. A. Ponomarenko, G. Falkovich, K. Watanabe, T. Taniguchi, I. V. Grigorieva, L. S. Levitov, M. Polini, and A. K. Geim, Superballistic flow of viscous electron fluid through graphene constrictions, Nat. Phys. **13**, 1182 (2017).
[32] J. A. Sulpizio, L. Ella, A. Rozen, J. Birkbeck, D. J. Perello, D. Dutta, M. Ben-Shalom, T. Taniguchi, K. Watanabe, T. Holder, R. Queiroz, A. Principi, A. Stern, T. Scaffidi, A. K. Geim, and S. Ilani, Visualizing Poiseuille flow of hydrodynamic electrons, Nature (London) **576**, 75 (2019).
[33] J. M. Schneider, M. Orlita, M. Potemski, and D. K. Maude, Consistent interpretation of the low-temperature magnetotransport in graphite using the Slonczewski-Weiss-McClure 3D band-structure calculations, Phys. Rev. Lett. **102**, 166403 (2009).
[34] T. Taen, K. Uchida, and T. Osada, Thickness-dependent phase transition in graphite under high magnetic field, Phys. Rev. B **97**, 115122 (2018).
[35] T. Taen, K. Uchida, T. Osada, and W. Kang, Tunable magnetoresistance in thin-film graphite field-effect transistor by gate voltage, Phys. Rev. B **98**, 155136 (2018).
[36] Y. Takada and H. Goto, Exchange and correlation effects in the three-dimensional electron gas in strong magnetic fields and application to graphite, J. Phys.: Condens. Matter **10**, 11315 (1998).
[37] B. Fauqué, D. LeBoeuf, B. Vignolle, M. Nardone, C. Proust, and K. Behnia, Two phase transitions induced by a magnetic field in graphite, Phys. Rev. Lett. **110**, 266601 (2013).
[38] K. Akiba, A. Miyake, H. Yaguchi, A. Matsuo, K. Kindo, and M. Tokunaga, Possible excitonic phase of graphite in the quantum limit state, J. Phys. Soc. Jpn. **84**, 054709 (2015).
[39] S. Tanuma, R. Inada, A. Furukawa, O. Takahashi, Y. Iye, and Y. Onuki, Electrical properties of layered materials at high magnetic fields, in *Physics in High Magnetic Fields*, edited by S. Chikazumi and N. Miura (Springer Berlin Heidelberg, Berlin, Heidelberg, 1981), pp. 316–319.
[40] H. Yaguchi and J. Singleton, Field-induced reentrant electronic phase transitions in graphite, Phys. B: Condens. Matter **256-258**, 621 (1998).
[41] H. Yaguchi and J. Singleton, A high-magnetic-field-induced density-wave state in graphite, J. Phys.: Condens. Matter **21**, 344207 (2009).
[42] Y. Cao, V. Fatemi, A. Demir, S. Fang, S. L. Tomarken, J. Y. Luo, J. D. Sanchez-Yamagishi, K. Watanabe, T. Taniguchi, E. Kaxiras, R. C. Ashoori, and P. Jarillo-Herrero, Correlated insulator behaviour at half-filling in magic-angle graphene superlattices, Nature (London) **556**, 80 (2018).
[43] Y. Cao, V. Fatemi, S. Fang, K. Watanabe, T. Taniguchi, E. Kaxiras, and P. Jarillo-Herrero, Unconventional superconductivity in magic-angle graphene superlattices, Nature (London) **556**, 43 (2018).
[44] A. L. Sharpe, E. J. Fox, A. W. Barnard, J. Finney, K. Watanabe, T. Taniguchi, M. A. Kastner, and D. Goldhaber-Gordon, Emergent ferromagnetism near three-quarters filling in twisted bilayer graphene, Science **365**, 605 (2019).
[45] F. Nihey and K. Nakamura, Aharonov-Bohm effect in antidot structures, Phys. B: Condens. Matter **184**, 398 (1993).
[46] R. Yagi, M. Shimomura, F. Tahara, H. Kobara, and S. Fukada, Observing Altshuler–Aronov–Spivak oscillation in a hexagonal antidot array of monolayer graphene, J. Phys. Soc. Jpn. **81**, 063707 (2012).
[47] W.-T. Pong and C. Durkan, A review and outlook for an anomaly of scanning tunnelling microscopy (STM): Superlattices on graphite, J. Phys. D: Appl. Phys. **38**, R329 (2005).
[48] C. W. Rischau, S. Wiedmann, G. Seyfarth, D. LeBoeuf, K. Behnia, and B. Fauqué, Quantum interference in a macroscopic van der Waals conductor, Phys. Rev. B **95**, 085206 (2017).
[49] K. Nakao, Landau level structure and magnetic breakthrough in graphite, J. Phys. Soc. Jpn. **40**, 761 (1976).

[50] O. E. Raichev, Magnetic oscillations of resistivity and absorption of radiation in quantum wells with two populated subbands, Phys. Rev. B **78**, 125304 (2008).

[51] I. A. Dmitriev, A. D. Mirlin, D. G. Polyakov, and M. A. Zudov, Nonequilibrium phenomena in high Landau levels, Rev. Mod. Phys. **84**, 1709 (2012).

[52] I. Y. Phinney, D. A. Bandurin, C. Collignon, I. A. Dmitriev, T. Taniguchi, K. Watanabe, and P. Jarillo-Herrero, Strong interminivalley scattering in twisted bilayer graphene revealed by high-temperature magneto-oscillations, Phys. Rev. Lett. **127**, 056802 (2021).